

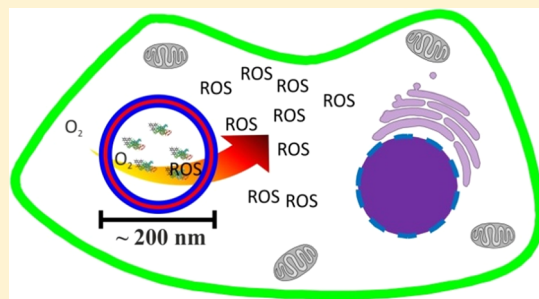
# Cellular Trojan Horse Based Polymer Nanoreactors with Light-Sensitive Activity

Patric Baumann, Mariana Spulber, Ionel Adrian Dinu, and Cornelia G. Palivan\*

Chemistry Department, University of Basel, Klingelbergstrasse 80, Basel, Switzerland

Supporting Information

**ABSTRACT:** Stimulus-sensitive systems at the nanoscale represent ideal candidates for improving therapeutic and diagnostic approaches by producing rapid responses to the presence of specific molecules or conditions either by changing properties or by acting “on demand”. Here we introduce an optimized light-sensitive nanoreactor based on encapsulation of a photosensitizer inside polymer vesicles to serve as an efficient source of reactive oxygen species (ROS) “on demand”. Two types of amphiphilic block copolymers, poly(2-methyloxazoline)-block-poly(dimethylsiloxane)-block-poly(2-methyloxazoline), PMOXA-PDMS-PMOXA, and poly(*N*-vinylpyrrolidone)-block-poly(dimethylsiloxane)-block-poly(*N*-vinylpyrrolidone), PNVP-PDMS-PNVP, were used to encapsulate Rose Bengal-bovine serum albumin (RB-BSA) inside the cavity of vesicles. The difference of copolymers molecular properties (hydrophobic to hydrophilic ratio, different chemical nature of the hydrophilic block) influenced the encapsulation ability, and uptake by cells, allowing therefore a selection of the most efficient polymer system. Nanoreactors were optimized in terms of (i) size, (ii) stability, and (iii) encapsulation efficiency based on a combination of light scattering, TEM, and UV-vis spectroscopy. By illumination, encapsulated RB-BSA conjugates generated *in situ* ROS, which diffused through the polymer membrane to the environment of the vesicles, as proved by electron spin resonance spectroscopy (ESR). Optimum illumination conditions were obtained based on the effect of the illumination time on the amount of ROS produced *in situ* by the encapsulated RB-BSA conjugates. ROS diffusion monitored by ESR was dependent on the molecular weight of copolymer that influences the thickness of the polymer membrane. Upon uptake into HeLa cells our nontoxic nanoreactors acted as a Trojan horse: they produced illumination-controlled ROS in sufficient amounts to induce cell death under photodynamic therapy (PDT) conditions. Straightforward production, stability, and Trojan horse activity inside cells support our light-sensitive nanoreactors for medical applications which require ROS to be generated with precise time and space control.



## INTRODUCTION

In response to challenges of modern medicine, such as increasing the efficacy of drugs while decreasing their side effects, improving detection limits of pathologic situations, or providing simultaneous detection and treatment, nanoscience is generating new systems and approaches.<sup>1–3</sup> In this respect, 3D supramolecular assemblies with sizes in the nanometer range, such as micelles, dendrimers, liposomes, nanoparticles, or polymersomes, are being developed with the aim of improving therapeutic and diagnostic approaches by encapsulation/entrapment of active molecules inside their structures.<sup>3,4</sup> They can be used as nanocarriers for improving drug delivery due to the shielding effect of their 3D assemblies and produce an improvement in the “enhanced permeability and retention” effect.<sup>5</sup>

Nanocarriers have been introduced to improve the efficacy of photodynamic therapy (PDT), a therapeutic strategy that applies reactive oxygen species (ROS) to combat pathologic situations, such as cancer.<sup>6</sup> ROS, produced by photosensitizer molecules upon irradiation with electromagnetic radiation, induce damage to the plasma membrane and DNA and as the

ultimate target cell death.<sup>7</sup> Although most approved photosensitizers are aimed at and optimized for precancerous and cancerous lesions,<sup>8</sup> they may also be used for antimicrobial purposes.<sup>9,10</sup> However, their effects are still limited by low water solubility and correspondingly low cellular uptake, and new approaches to increase intracellular delivery of photosensitizers are still needed,<sup>11</sup> especially in the case of treatment of endoscopic accessible tumors.<sup>12</sup> In this respect, nanocarriers can increase the intracellular delivery of photosensitizers by entrapping them inside 3D supramolecular assemblies, which also decreases their intrinsic toxicity.<sup>6</sup> However, a major drawback of nanocarriers is the uncontrolled release of the entrapped molecules into biological compartments other than the desired ones, leading to post-treatment side effects and lower PDT efficiency.<sup>13</sup>

Nanoreactors are ideal candidates for providing efficient solutions for treatment of pathologic situations, as for example

Received: May 26, 2014

Revised: July 17, 2014

Published: July 21, 2014



via PDT. Polymer nanoreactors are 3D supramolecular assemblies that contain encapsulated/trapped active molecules, such as enzymes, proteins, and small molecular mass catalysts, protected from environmental conditions, and able to act only *in situ*.<sup>14</sup> In particular, polymer vesicles have been successfully used to generate nanoreactors, which, because of their simple and mild engineering conditions, preserve the activity of the active molecule, while preventing its release from the polymer assembly.<sup>15</sup> The *in situ* activity of encapsulated molecules is supported by a polymer membrane, which allows the transport of substrates and products.<sup>16</sup> Based on this intrinsic property of allowing a specific reaction *in situ* for the production of particular products, such as prodrugs,<sup>17</sup> antibiotics,<sup>18</sup> and free radicals,<sup>19</sup> nanoreactors can be designed to act as cellular implants. Depending on the specificity of the reaction taking place in the nanoreactor compartment, it is possible to create artificial organelles<sup>20</sup> or biosensors for detection of molecules relevant to pathological conditions.<sup>14</sup>

A nanoreactor, which transports a particular encapsulated/trapped compound to an intended biological location and then produces an active substance in the presence of a stimulus, can be considered as a cellular Trojan horse. In order to generate a cellular Trojan horse, a complex scenario of requirements has to be fulfilled: (i) sufficient stability to protect and preserve an active compound, (ii) act only when the appropriate stimulus is present, and (iii) fulfill its function only upon uptake into cells.

On the basis of encapsulating a photosensitizer inside polymer vesicles, we previously introduced a polymer nanoreactor, which is able to function as an intracellular source of ROS when irradiated with electromagnetic radiation of appropriate wavelength.<sup>19</sup> Upon irradiation the nanoreactor generates singlet oxygen, which passes through the vesicle membrane, which is selected to be permeable to ROS,<sup>21,22</sup> and the increased intracellular level of ROS induces cell death.<sup>23</sup> Here, we take this concept a step further by optimizing this type of nanoreactor to serve as an efficient cellular Trojan horse with the ability to induce cell death “on demand” in conditions specific to photodynamic therapy (Figure 1).

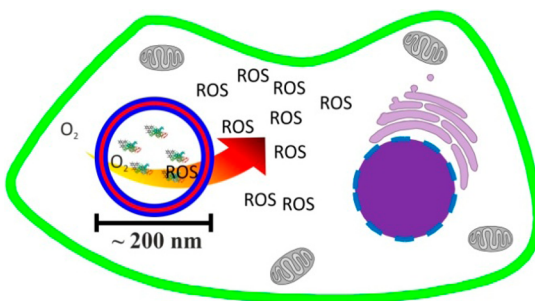


**Figure 1.** Schematic representation of a light-responsive nanoreactor containing photosensitizers to act as a cellular Trojan horse by producing ROS inside cells “on demand”.

This uses Rose Bengal conjugated with bovine serum albumin (RB–BSA) encapsulated inside the cavity of PMOXA–PDMS–PMOXA and PNVP–PDMS–PNVP vesicles. To obtain an efficient ROS source, which can be shut on/off with precise time and space resolution, the nanoreactor was optimized to simultaneously fulfill a complex scenario of requirements: (i) an increased encapsulation efficiency, (ii) a rapid ROS release upon production, (iii) an

extended wavelength range of electromagnetic radiation for activation into the visible domain, and (iv) an improved uptake inside cells. We systematically varied molecular parameters, such as chemical nature of the hydrophilic block, hydrophobic-to-hydrophilic ratio, and size of polymer vesicles in order to improve the encapsulation efficiency, the membrane permeability for ROS, and the uptake. In addition, the amount of encapsulated photosensitizer and the irradiation conditions were adjusted to cope with the specificity of photodynamic therapy applications. Besides, we were interested in understanding the relationship between the irradiation time of the nanoreactor, the level of ROS produced, and cell viability. In this respect, we identified and quantified the main secondary radicals produced upon illumination of nanoreactors taken up by HeLa cells. A spin trap active only in intracellular compartment was used to directly quantify the level of secondary radicals produced by the Trojan horse inside cells, based on the formation of a stable nitroxide radical detectable by electron spin resonance (ESR).<sup>24</sup> In addition, we assessed the permeability of the polymer membrane to ROS, which is a key factor in the efficient release of ROS into the vesicle environment. The effect of the molecular properties of the copolymer on ROS diffusion was monitored by spin trap ESR. Uptake and cell viability assays were used to evaluate the efficacy of nanoreactors to act as cellular Trojan horses.

The concept of an efficient Trojan horse, which has been described here for PDT, can be easily expanded to other applications in which the production of a specific compound is necessary with a precise time scale and location by changing the encapsulated active compound. Trojan horses are expected to offer smart solutions to various pathologic conditions by producing a specific compound “on demand”.

## RESULTS AND DISCUSSION

An efficient cellular Trojan horse requires a rapid and local response to a specific stimulus: the desired reaction is activated only when the stimulus is present. Irradiation with electromagnetic radiation, for example with light provided by a light source, represents an efficient stimulus in terms of specificity, rapidity, and on/off function. If the compound encapsulated inside the polymer vesicles is activated by electromagnetic radiation of a specific wavelength, the system will act only when it is irradiated with the appropriate radiation.

Thus, the match between the compound inside polymer vesicles and the external stimulus is the key factor for modulating the function of the Trojan horse with spatial and temporal precision.

We selected Rose Bengal (RB), which is known to be an efficient photosensitizer, and produces ROS upon light irradiation.<sup>25</sup> The drawback of the hydrophobic character of RB was overcome by conjugation to BSA, which improved the encapsulation efficiency and avoided interaction with the membrane of the polymer vesicles. We used PMOXA–PDMS–PMOXA and PNVP–PDMS–PNVP copolymers for vesicle formation (see Table 1) because their polymer membranes are known to be permeable to oxygen species<sup>21,22</sup> but impermeable to larger molecules, such as water and urea.<sup>16</sup>

By encapsulating the photosensitizer BSA conjugate inside polymer vesicles, we addressed the key issues of (i) increasing the amount of photosensitizer located in a confined space and (ii) decreasing their intrinsic toxicity by the shielding effect of the polymer membrane.

**Table 1. Polymer Composition and Molecular Weight**

polymer	composition	$M_n$ / (GPC)	references
A1	PMOXA <sub>10</sub> –PDMS <sub>87</sub> –PMOXA <sub>10</sub>	8352	ref 19
A2	PMOXA <sub>14</sub> –PDMS <sub>33</sub> –PMOXA <sub>14</sub>	4720	Polymer Source P3691A
A3	PMOXA <sub>6</sub> –PDMS <sub>44</sub> –PMOXA <sub>6</sub>	4555	Supporting Information
B1	PNVP <sub>5.5</sub> –PDMS <sub>17</sub> –PNVP <sub>5.5</sub>	2360	ref 26
B2	PNVP <sub>8.5</sub> –PDMS <sub>17</sub> –PNVP <sub>8.5</sub>	4200	ref 26
B3	PNVP <sub>15</sub> –PDMS <sub>37</sub> –PNVP <sub>15</sub>	6160	ref 26

**Nanoreactor Generation and Characterization.** All nanoreactors were prepared using the film rehydration method in which a polymer film is hydrated with a solution containing the RB–BSA conjugate (50  $\mu\text{M}$ ).<sup>19</sup> To decrease the size distribution, all PDMS–PMOX–PDMS and PNVP–PDMS–PNVP supramolecular assemblies were extruded through a 0.2  $\mu\text{m}$  pore size membrane. In order to get more insights into the size effects of such supramolecular assemblies, the supramolecular assemblies based on A1 were additionally extruded through 0.1 and 0.05  $\mu\text{m}$  filters. The desired size for all nanoreactors was 50–200 nm to take advantage of enhanced permeability and retention, while being large enough to avoid renal clearance.<sup>27</sup> Supramolecular assemblies loaded with RB–BSA conjugates were compared with empty assemblies prepared under similar conditions.

The dimensions and architecture obtained by self-assembly of amphiphilic copolymers in the presence of RB–BSA conjugates were evaluated after extrusion using dynamic and static light scattering (Table 2). The ratio ( $\rho$ ) between the

**Table 2. Encapsulation Efficiency and Sizes of the Nanoreactors**

sample	$R_g$ [nm]	$R_h$ [nm]	encapsulation efficiency [%]	RB–BSA conjugate per vesicle
A1-200 <sup>a</sup>	103	109	13.0	22
A1-100 <sup>a</sup>	70	74	13.0	7
A1-50 <sup>a</sup>	55	60	13.0	4
A2	89	95	2.3	2
A3	149	157	12.5	61
B1	120	118	1.5	3
B2	112	121	3.8	13
B3	118	129	8.6	23

<sup>a</sup>A1 supramolecular assemblies were extruded through filters with a pore size of 200  $\mu\text{m}$  (A1-200), 200 and then 100  $\mu\text{m}$  (A1-100), and 200 and then 50  $\mu\text{m}$  (A1-50).

radius of gyration ( $R_g$ ) and the hydrodynamic radius ( $R_h$ ) was in all cases close to 1, which is the theoretical value for a perfect hollow sphere.<sup>28</sup> The size and the hollow nature of empty vesicles and nanoreactors were confirmed by TEM micrographs showing round and collapsed spherical objects (Figures S2a and S3–S5).

The RB–BSA encapsulation efficiency was calculated by comparing the initial RB–BSA concentration with that after nanoreactor formation and purification. The encapsulation efficiency of 1.5–13% is in agreement with similar polymer vesicles containing encapsulated proteins.<sup>17,18</sup> The maximum number of RB–BSA conjugates per nanoreactor that can be encapsulated by the self-assembly process of vesicles formation (for a concentration of RB–BSA of 6.5  $\mu\text{M}$ ) was estimated by

assuming an homogeneous distribution of conjugates in the solution prior to the self-assembly process, and neglecting the very small fraction of nonencapsulated RB–BSA, which was not removed by size exclusion (eq 2). As expected, the vesicles with the highest  $R_h$  allow the highest number of RB–BSA conjugates per vesicle for a similar initial amount of RB–BSA (6.5  $\mu\text{M}$ ) used for the encapsulation process.

Interestingly, encapsulation of RB–BSA conjugates was higher with PMOXA–PDMS–PMOXA based vesicles than with those based on PNVP–PDMS–PNVP copolymers. This is explained by a higher pH value used for the nanoreactor generation than the  $pK_a$  value of PNVP–PDMS–PNVP (around 6.8) and of BSA (4.7). These conditions induced an overall negative charge on both copolymer and RB–BSA conjugate, which decreased significantly the encapsulation efficiency due to electrostatic repulsion. As shown by ref 29 at pH 7.5, PNVP exhibits a negative zeta-potential ( $\xi$  –6 mV). The polarity of PNVP compared with PMOXA is due to accumulation of *n*-electrons on the carbonyl groups in vicinity of the tertiary amine group from PNVP molecules, as indicated in the literature.<sup>29</sup> On the contrary, PMOXA–PDMS–PMOXA copolymers being neutral, they serve for higher RB–BSA encapsulation efficiency. We increased the initial concentration of RB–BSA from 0.5 up to 10  $\mu\text{M}$  in order to get the highest encapsulation efficiency. 10  $\mu\text{M}$  RB–BSA used as starting amount for nanoreactors preparation represents the maximum concentration of RB–BSA which does not affect the self-assembly process<sup>19</sup> and therefore was used for all the other copolymer assemblies.

A key factor supporting the efficacy of nanoreactors for use as Trojan horses is their stability upon illumination, which was tested after illumination with 90 J/cm<sup>2</sup> by light scattering and TEM. The obtained radii and the presence of few collapsed structures indicated that illumination and induced ROS production had little effect on the vesicular structure (Table S2 and Figure S2b).

**Cellular Uptake of Nanoreactors.** In order to test their efficiency for acting as a Trojan horse, the uptake of nanoreactors into HeLa cells was assessed by flow cytometry (Figure 2). This was done by incubating HeLa cells with nanoreactors with high encapsulation efficiency (A1-, A3-, B2-, and B3-based nanoreactors) for 24 h.

Nanoreactors based on all copolymers were taken up within 24 h. The amount of RB–BSA conjugates per cell increased in

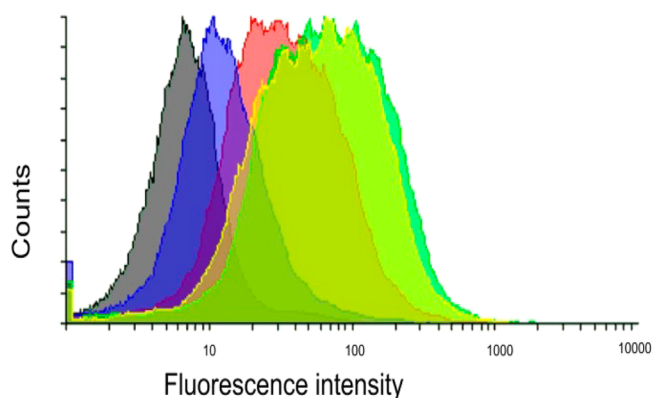


**Figure 2.** Flow cytometry: cells incubated with A1-200 (green), A3 (yellow), B2 (blue)- and B3 (red) nanoreactors and control cells (black).

the order B2- < B3- < A3- < A1-based vesicles, as observed by the shift in the fluorescence signals in the flow cytometry histograms. According to the flow cytometry experiment, PMOXA-PDMS-PMOXA based vesicles are better taken up than PNVP-PDMS-PNVP vesicles. This is in agreement with the encapsulation efficiency of nanoreactors: a higher uptake is observed for nanoreactors with higher encapsulation efficiency, closely related to the chemical nature of the hydrophilic block of copolymers. In addition, for the same chemical nature of copolymers (PMOXA-PDMS-PMOXA), the size of vesicles is the key factor influencing the uptake behavior: vesicles with radius lower than 120 nm present an improved uptake (A1), than those with higher diameter (A3), while they have almost similar encapsulation efficiency (Table 2). LSM micrographs of cells incubated with A1-based nanoreactors with different sizes (A1-200, A1-100, and A1-50) support the fact that the radius of vesicles in the range of 50–120 nm does not influence uptake behavior (Figure S6).

The optimization of nanoreactors with respect to encapsulation efficiency and uptake behavior indicates that PMOXA-PDMS-PMOXA vesicles with radius lower than 120 nm provide an efficient Trojan horse. Therefore, these nanoreactors were further tested inside cells to get insight into their functionality as Trojan horse.

**Characterization of ROS Produced by Illuminated Trojan Horses.** In order to investigate the relative concentration of reactive oxygen species generated by A1-based nanoreactors, and their ability to diffuse through the polymer membrane, we used ESR spin trapping with 5,5-dimethyl-1-pyrroline-N-oxide (DMPO). With illumination of RB-BSA, various secondary reactive oxygen species are formed (e.g., superoxide radical anion and hydroxyl radical). The intensity of ESR signal resulting from the spin trapping of hydroxyl radicals with DMPO<sup>30</sup> was used to compare the level of ROS released from the nanoreactor to that generated by free RB-BSA. The comparison serves for predicting the Trojan horse efficiency.

First, we identified the ROS generated by RB-BSA on bulk illumination and then compared them with the ROS that were released from the nanoreactor when illuminated under similar conditions. Identical amounts of free and encapsulated RB-BSA were illuminated with a daylight simulating light plate with an intensity of 50 mW/cm<sup>2</sup> in the presence of the same concentrations of DMPO (0.75 mM), and the ESR spectra of the corresponding spin adducts were recorded at room temperature. On illumination of free RB-BSA, only one ESR signal was observed (Figure 3A) with hyperfine coupling constants  $a_N = 14.9$  G and  $a_H = 14.9$  G, characteristic of a DMPO/OH adduct.<sup>30</sup> As the lifetime of DMPO superoxide adduct is very short (<1 min),<sup>31</sup> it is possible that other reactive species were formed but not detected on the experimental time scale. When nanoreactors were illuminated in the presence of DMPO, the same DMPO/OH adducts (with  $a_N = 14.9$  G and  $a_H = 14.9$  G) were observed (Figure 3B) along with an additional small contribution (<5%) from a spectrum typical of a DMPO adduct of a carbon-centered radical. The relative intensity of the ESR spectrum of DMPO/OH adducts was higher for encapsulated RB-BSA than with free RB-BSA, and no ESR signal was detected when empty A1-200-based vesicles were illuminated in the same conditions in the presence of DMPO (Figure 3B, A1-200).

The total spin count value determined by SpinCount and Bruker internal standards ranged from  $2.5 \times 10^{10}/\text{mm}^3$  for free

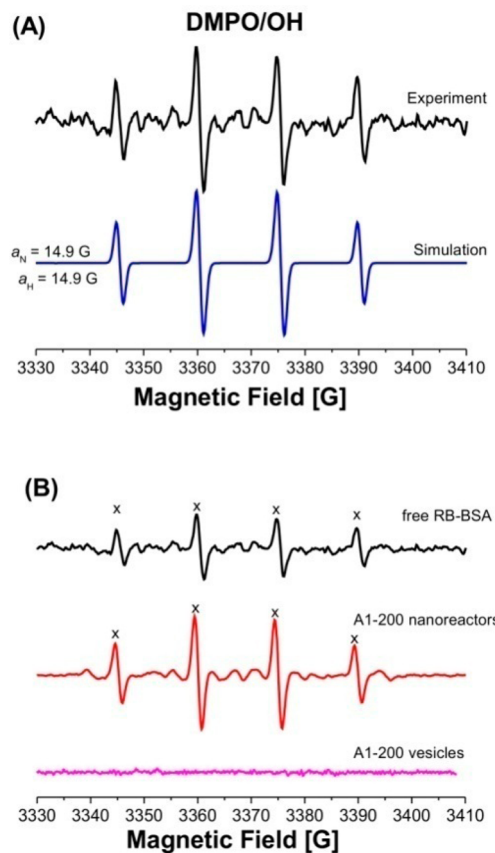


**Figure 3.** (A) Experimental and simulated ESR spectra of DMPO/OH adducts formed in the presence of illuminated free RB-BSA. (B) Experimental ESR spectra of DMPO/OH adducts (marked with X) formed by DMPO in the presence of free RB-BSA (black line) and RB-BSA nanoreactors (A1-RB-BSA red line). The samples were illuminated for 10 min ( $30 \text{ J}/\text{cm}^2$ ).

RB-BSA to  $9.74 \times 10^{10}/\text{mm}^3$  for nanoreactors (Figure 3B). The total spin count value reflects the total amount of DMPO/OH adducts formed in the system upon illumination (free RB-BSA in bulk and RB-BSA inside nanoreactors). The ratio between these values represents the relative amount of ROS resulting upon illumination of RB-BSA and indicates that encapsulated photosensitizer has a significantly higher efficiency for ROS generation than free photosensitizer. The increase in spin adducts intensity is explained by the higher local concentration of RB-BSA inside the nanoreactors. In addition, these results indicate rapid diffusion of ROS through the polymer membrane, in agreement with previous reports on ROS permeability of membranes based of these types of amphiphilic block copolymers, but with different hydrophobic-to-hydrophilic ratios.<sup>32</sup>

In the absence of illumination, no DMPO adducts were detected with either empty A1-200-based polymer vesicles or the corresponding nanoreactors. Longer illumination times (25–30 min) ( $30\text{--}75 \text{ J}/\text{cm}^2$ ) led to an increased amount of the C-centered radicals adducts. This indicates that the illumination time has an important role in improving the efficiency of RB-BSA loaded nanoreactors. In addition, similar DMPO spin trapping experiments performed with RB-BSA containing A2- and A3-nanoreactors indicated no DMPO/OH signal, but the formation of DMPO/C-centered adducts. Higher molecular

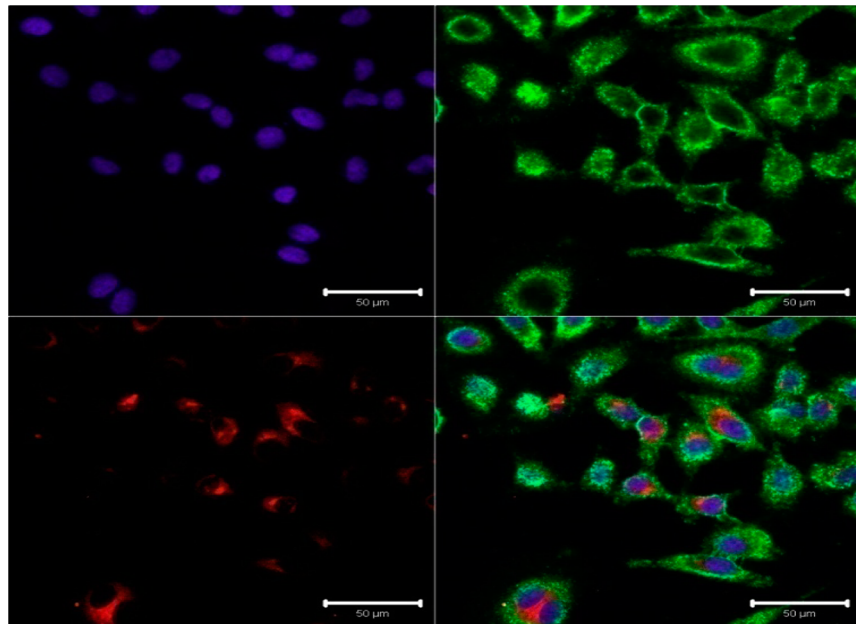


**Figure 4.** HeLa cells incubated for 24 h with doxorubicin-containing vesicles. Violet channel: Hoechst DNA staining; green channel: cell mask deep red staining; red channel: doxorubicin-loaded vesicles (scale bar 50  $\mu$ m).

mass of the copolymer increased the membrane thickness and therefore its mechanical stability.

**In Vitro Stability Studies of Nanoreactors.** An essential requirement to decrease possible side effects is the stability of nanoreactors inside cells, until the light is applied to activate it. To investigate the stability of the polymer vesicles inside cells, as an essential requirement for a functional Trojan horse, we encapsulated doxorubicin (DOX) in polymer vesicles because its release in the case of vesicle degradation can be followed *in situ* in cells. Free DOX intercalates with DNA in the cell, and its signal then overlays that of the DNA staining signal.<sup>33</sup> As the fluorescence signal of DOX did not overlay the nuclei fluorescence signal, there was no intercalation between the DNA and DOX in the case of our DOX-loaded vesicles (Figure 4), a result which indicates that the loaded vesicles preserved their architecture inside cells for at least 24 h. As in Rose Bengal clinical studies the time between the administration of the photosensitizer, irradiation process, and ROS generation is limited to several hours,<sup>34</sup> our system fulfills the stability condition to ensure the viability of a PDT treatment. The stability of A1-200-based vesicles inside cells was expected because vesicles of similar amphiphilic copolymers remained intact for more than 48 h.<sup>35</sup>

**Functionality of the Optimized Nanoreactor Containing RB-BSA as Cellular Trojan Horse.** To establish the functionality of RB-BSA-containing vesicles as a cellular Trojan horse, we followed the intracellular radical production of the nanoreactor by examining cell viability with the MTS assay (Figure 5).<sup>19</sup> HeLa cells were incubated with RB-BSA nanoreactors and washed after 24 h. After washing and medium exchange, the cells were homogeneously illuminated for 0–30 min with an artificial daylight lamp (0–90 J/cm<sup>2</sup>), with intensity in the normal range used medically for PDT.<sup>36</sup> Nonilluminated cells stayed almost as healthy as those grown without nanoreactors, and the small decrease in viability can be explained by the oxidative stress induced by the uptake of nanoreactors,<sup>37</sup> as already reported with nanoreactors based on this type of amphiphilic block copolymer.<sup>19</sup>

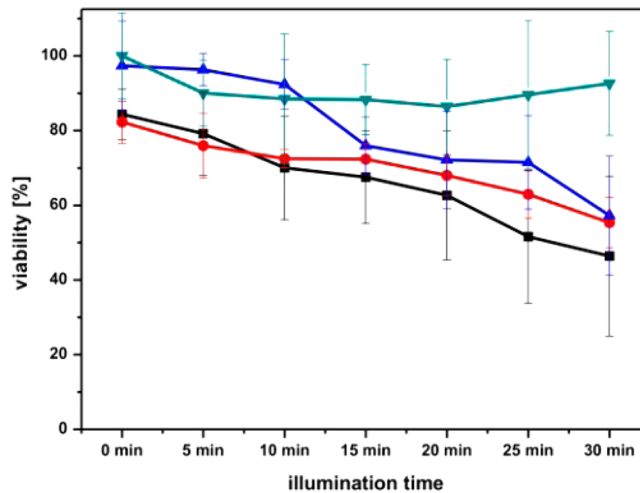


**Figure 5.** MTS assay of HeLa cells incubated with nanoreactors of different size illuminated for different periods of time: (▼) control cells without nanoreactors; (▲) A1-50-based nanoreactors; (●) A1-100-based nanoreactors; (■) A1-200-based nanoreactors.

Upon illumination, the ROS levels in cells increased because of ROS production by the RB-BSA nanoreactors.<sup>19</sup> The viability of cells incubated for 24 h with A1-200-based nanoreactors dropped below 50%, while those of cells incubated with A1-100- or A1-50-based nanoreactors were reduced to <60%. The light applied to the cells in order to activate the Trojan horse only slightly affected cell viability, as expected for the specific illumination conditions used (Figure 5). The viability of cells with and without nanoreactors was unchanged in the dark.

Reduced viability of cells upon incubation with Trojan horses is also indicated by LSM micrographs after illumination with the same light intensity (75 J/cm<sup>2</sup>). Illuminated nanoreactors induced bleb formation (Figure 6), which is typical for cells treated by photodynamic therapy, and indicates apoptosis.<sup>7</sup> The dose of RB-BSA encapsulated in nanoreactors is around 1.3

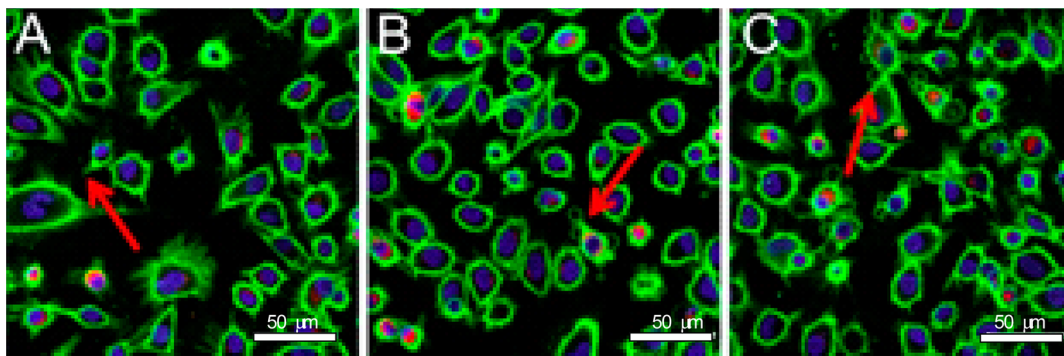


**Figure 6.** HeLa cells incubated with Trojan horses based on vesicles with different  $R_h$ : (A) 50, (B) 100, and (C) 200 nm. Illumination time 25 min ( $75 \text{ J/cm}^2$ ). The arrows indicate the presence of blebs.

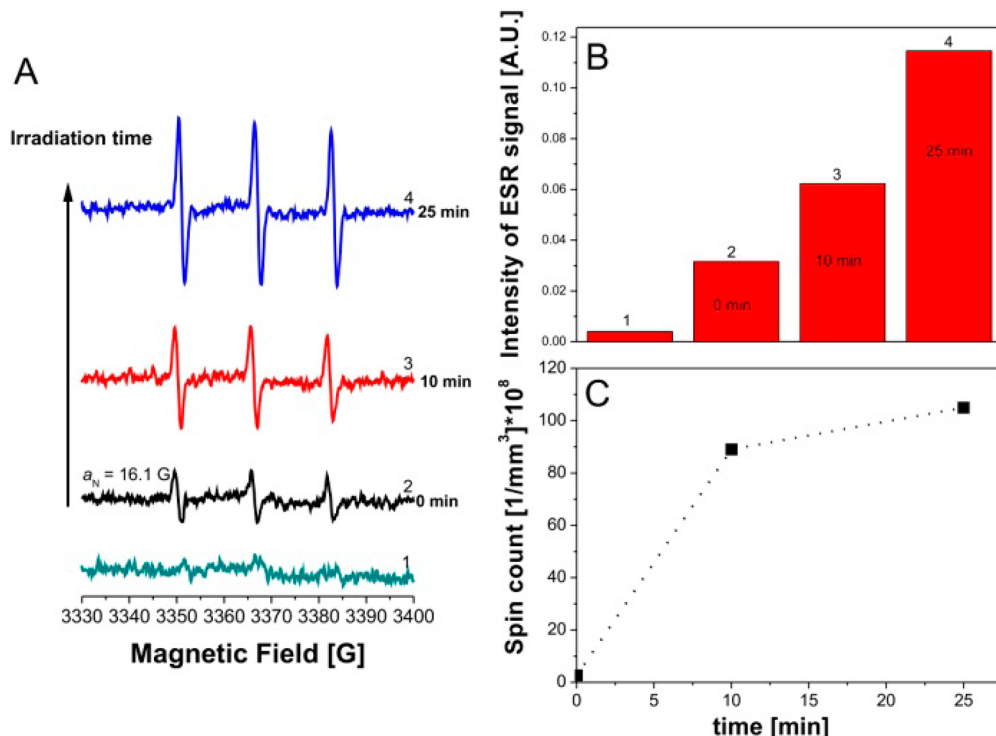


**Figure 7.** (A) ESR spectra of typical nitroxide signal formed by incubating ACP with cells (1) and cells incubated with A1-200-based nanoreactors for different illumination times (0–25 min) (2–4). (B) Intensity of the nitroxide ESR signal generated when cells were incubated with ACP in the absence (1) and in the presence of A1-200-based nanoreactors for different irradiation times (2–4). (C) Spin counts for nitroxide radicals formed in the presence of RB-BSA loaded A1-200-based nanoreactors in the dark and after 10 and 25 min illumination.

$\mu\text{M}$ , more than 100 times smaller than the commonly used doses (200–300  $\mu\text{M}$ ).<sup>38</sup> This indicates a high efficacy of our Trojan horse, which allows a significant decrease of photosensitizer dose by encapsulation inside vesicles, while producing a high ROS amount to support PDT.

To get more insight into the Trojan horse activity, the intracellular ROS levels were measured by spin trapping ESR. HeLa cells containing nanoreactors were rinsed with PBS and treated before illumination with acyl-protected hydroxylamine ACP, a spin probe already used for estimation of the intracellular oxidative stress.<sup>24</sup> Although ACP is stable outside cells because of protection from its acyl groups, inside cells it is deprotected by the esterase activity and oxidized in the presence of cellular ROS to a stable nitroxide, which is easily detected by ESR.

A weak ESR spectrum, characteristic of a nitroxide radical ( $a_N = 16.1 \text{ G}$ ), was detected when cells were incubated with ACP (Figure 7) as a result of oxidation of ACP by ROS naturally occurring in HeLa cells. When cells were incubated in the presence of 100  $\mu\text{g}/\text{mL}$  A1-200 nanoreactors in the dark, the intensity of the ESR spectrum was increased slightly due to oxidative stress generated by vesicle uptake and in agreement with viability results.<sup>39</sup> However, the level of ROS generated by the uptake of the nanoreactors is not in a toxic range. Even a high concentration of polymer vesicles (up to 300 mg/mL) in the culture medium did not lead to higher cytotoxicity.<sup>19,35</sup>

Cells incubated with ACP or with nanoreactors plus ACP showed a considerable increase in the nitroxide ESR signal after 10 min illumination, reaching a maximum after 25 min illumination (Figure 7). Spin counts increased from  $2.65 \times 10^8/\text{mm}^3$  total spins for cells incubated with A1-200-based

nanoreactors in the dark to  $8.9 \times 10^9/\text{mm}^3$  for nanoreactors after 10 min irradiation and  $1.05 \times 10^{10}/\text{mm}^3$  after 25 min irradiation, respectively. The significant increase in spin counts upon illumination indicates the efficiency of the nanoreactor to function as a Trojan horse. Within 25 min illumination, the level of ROS in HeLa cells was increased by a factor of 40 (Figure 7).

The increased amounts of ROS detected on illumination of nanoreactors containing BR–BSA together with their stability inside cells demonstrate their function as an efficient Trojan horse, which prevents the release of the photosensitizer, while functioning as a successful source of ROS “on demand”. In addition, ROS are generated with high time and space precision due to the confinement of the photosensitizer inside the nanoreactors and the use of light as stimulus.

The increased amounts of ROS detected on illumination of nanoreactors containing RB–BSA together with their stability inside cells demonstrates their function as an efficient Trojan horse, which prevents the release of the photosensitizer, while functioning as a successful source of ROS “on demand”. In addition, ROS are generated with high time and space precision due to the confinement of the photosensitizer inside the nanoreactors and the use of light as stimulus.

## CONCLUSIONS

We successfully developed a cellular Trojan horse that acts as a source of ROS “on demand” inside cells. The Trojan horse was engineered by optimizing a light responsive nanoreactor based on a highly active photosensitizer encapsulated in polymer vesicles. Upon illumination, ROS passed through the polymer membrane of the vesicles, which were especially designed to be permeable to ROS. We systematically optimized various parameters such as size of vesicles, encapsulation efficiency, irradiation conditions, and the uptake by HeLa cells to produce an efficient ROS source inside cells for the induction of apoptosis.

Two different amphiphilic block copolymers (PMOXA–PDMS–PMOXA and PNVP–PDMS–PNVP) were used to form the nanoreactors by the self-assembly process in the presence of the RB–BSA conjugate. Nanoreactors based on PMOXA–PDMS–PMOXA vesicles with diameters of around 200 nm were the most efficient in terms of RB–BSA encapsulation and size to fulfill the requirements for high retention and permeability. These nanoreactors also had the highest uptake and stability in HeLa cells. While nontoxic in dark conditions, they produced ROS upon illumination in conditions specific for PDT. Intracellular ROS levels increased by a factor of 40, which was sufficient to significantly reduce cell viability in the region containing illuminated nanoreactors.

Our light-sensitive nanoreactors containing photosensitizers represents a straightforward approach to transport high amounts of photosensitizers into cells under safe conditions and to serve as a ROS sources “on demand” to induce cell death with time and space controlled precision. As the optimization process lead to identifying all the conditions in which the nanoreactors work, further *in vivo* experiments are planned.

## MATERIALS AND METHODS

**Materials.** Chemicals were obtained from Sigma-Aldrich and Invitrogen at the highest purity available and were used as received. A2 PMOXA–PDMS–PMOXA was purchased from

Polymer Source Inc. (Canada) 1-Acetoxy-3-carbamoyl-2,2,5,5-tetramethylpyrrolidine (ACP) and 5,5-dimethyl-1-pyrroline N-oxide (DMPO) were purchased from Enzo Life Sciences, Switzerland, and used without further treatment. A3 PDMS<sub>6</sub>–PMOXA<sub>44</sub>–PDMS<sub>6</sub> was synthesized according to refs 40 and 41 with certain modifications, as highlighted in the Supporting Information. B1 PNVP<sub>5.5</sub>–PDMS<sub>17</sub>–PNVP<sub>5.5</sub>, B2 PNVP<sub>8.5</sub>–PDMS<sub>17</sub>–PNVP<sub>8.5</sub>, and B3 PNVP<sub>15</sub>–PDMS<sub>37</sub>–PNVP<sub>15</sub> were synthesized as reported in the literature and were characterized by <sup>1</sup>H NMR and GPC.<sup>22</sup>

<sup>1</sup>H NMR PNVP<sub>5.5</sub>–PDMS<sub>17</sub>–PNVP<sub>5.5</sub> (400.1 MHz, CDCl<sub>3</sub>) δ/ppm = 3.7–3.85 (CH<sub>2</sub>–CH–N), 3.0–3.2 (CH<sub>2</sub>–CH<sub>2</sub>–N–CO), 2.7–3.0 (CH<sub>2</sub>–CH<sub>2</sub>–CONH) 2.3–2.4 (CH<sub>2</sub>–CH<sub>2</sub>–CH<sub>2</sub>–CO), 1.5–2.0 (CH<sub>2</sub>–CH–N–CO, CH<sub>2</sub>–CH<sub>2</sub>–CH<sub>2</sub>–CO, CH<sub>2</sub>–CH<sub>2</sub>–CONH, CH<sub>2</sub>–CH<sub>2</sub>–C, CH<sub>2</sub>–CH<sub>2</sub>–C, CH<sub>2</sub>–CH<sub>2</sub>–C(CH<sub>3</sub>)–CN), 1.45–1.50 ppm (CH<sub>2</sub>–CH<sub>2</sub>–CH<sub>2</sub>), 0.54 (m, –SiCH<sub>2</sub>), 0.1 (Si–(CH<sub>3</sub>)<sub>2</sub>).

A3: <sup>1</sup>H NMR (400 MHz, CDCl<sub>3</sub>) δ/ppm = 3.90–3.30 (bm, 12H), 2.30–2.00 (bm, 6H), 1.65–1.45 (bm, 4H), 0.55–0.40 (m, 4H), 0.25–0.0 (bs, 3H) (Figure S1).

**Preparation of RB–BSA Conjugates.** RB–BSA conjugates were prepared as described by Baumann et al.<sup>21</sup> Briefly, 300 μM BSA was dissolved in a PBS buffer containing 100 μM RB, and after 1 h at room temperature, the solution was applied to a HiTrap Desalting column containing SephadexTM Superfine (GE Healthcare, UK).

**Nanoreactor Preparation.** For vesicles formation the film rehydration method was used.<sup>19</sup> Briefly, 5 mg of polymer was dissolved in EtOH and dried under vacuum to form a polymer film on the inner bottom of a glass flask. The polymer film was rehydrated with PBS at 4 °C for 24 h in the presence or absence of the RB–BSA conjugate and then extruded through a 0.2 μm Nucleopore Track-Etch membrane from Whatman. Supramolecular assemblies generated by A1 copolymers were additionally extruded through a 100 and 50 nm membranes.

**Encapsulation Efficiency Calculation.** The process encapsulation efficiency (EE) was calculated as indicated in<sup>18</sup>

$$\text{EE [\%]} = \frac{\text{conc after encapsulation and purification}}{\text{conc before encapsulation}} \times 100 \quad (1)$$

The maximum number of RB–BSA conjugates (#RB–BSA<sub>per vesicle</sub>), which can be encapsulated per vesicle was calculated using<sup>42</sup>

$$\# \text{RB–BSA}_{\text{per vesicle}} = C_0 \times N_A \times 4/3 \times \pi \times R_h^3 \times 1000 \quad (2)$$

where  $C_0$  is the concentration of RB–BSA conjugates encapsulated [mol/L] and  $R_h$  is the hydrodynamic radius of vesicles [m] obtained from light scattering.

**ESR Sample Preparation for ROS Spin Trapping.** Each sample was prepared by mixing 0.1 mL of free or encapsulated RB–BSA with 0.3 mL of 1 mM DMPO. RB–BSA was diluted to obtain the same concentration (determined by UV-vis measurement at  $\lambda = 560$  nm) as encapsulated in nanoreactors.

**In Vitro ROS Assessment.** Cell culturing was adapted from Serrander et al.<sup>43</sup> 2 × 10<sup>5</sup> HeLa cells per well were cultured in Dulbecco's Modified Eagle's Medium (DMEM) containing 10% fetal calf serum (FCS) in a six-well plate for 24 h at 37 °C in a humidified CO<sub>2</sub> incubator. Afterward, the cells were incubated for another 24 h in DMEM and the presence of the vesicles. Cells were washed twice with PBS and then incubated under dark conditions at room temperature for 90 min with 10 mM 1-acetoxy-3-carbamoyl-2,2,5,5-tetramethylpyrrolidine

(ACP) (Enzo Life Sciences, Switzerland). Then, the cells were detached and centrifuged at 1000 rpm for 5 min; the supernatant removed, resuspended in 200  $\mu\text{L}$  of PBS, and finally transferred to a glass pipet for ESR measurement. The solutions containing ACP, cells, cells and ACP, cells and RB-BSA-containing nanoreactors were measured by ESR as prepared, before and after 5–20 min illumination with up to 75 J/cm<sup>2</sup>. Quantitative determination of unpaired electrons was performed using the SpinCount software and an internal reference provided by Bruker.

**HeLa Cell Viability Assay.** HeLa cells were cultured at a density of  $2 \times 10^4$  cells per well in a clear 96-well plate for 24 h. Cells then were incubated for another 24 h in the presence of RB-BSA loaded or empty vesicles. Afterward, the medium was removed and the cells were washed with PBS and fresh medium was given to the cells. The cells were illuminated in the incubator from the bottom for 0–30 min. Afterward, the MTS assay (Promega) was performed to measure cell viability, whereas the control cells with no illumination was set to 100% viability.

**In Vitro Stability of Nanoreactors.** Vesicles were formed in the presence of 100  $\mu\text{M}$  doxorubicin HCl in PBS and purified as described above. HeLa cells were cultured as described above and incubated for 24 h with 100 mg/mL nanoreactor containing doxorubicin. Cells were washed, stained, and recorded as described above, and the fluorescence signal of doxorubicin instead of RB-BSA was recorded in channel 3.

**Methods.** Dynamic and static light scattering measurements were performed using an ALV goniometer (ALV GmbH, Germany) equipped with an ALV HeNe laser (JDS uniphase,  $\lambda = 632.8$  nm). The vesicle solution (0.33–1 mg/mL) was measured in a 10 mm cylindrical quartz cell at angles ranging from 30° to 150° at 293 K and processed using ALV/Static & Dynamic FIT and PLOT program version 4.31 10/10. Static light scattering data were processed according to the Berry model.

**Transmission Electron Microscopy.** 10  $\mu\text{L}$  of nanoreactor solution was negatively stained with 2% uranyl acetate solution, deposited on a carbon-coated copper grid, and then examined with a transmission electron microscope (Philips Morgani 268 D) operated at 80 kV.

**UV-vis Spectroscopy.** The RB-BSA concentration was determined by UV-vis spectroscopy ( $\lambda = 560$  nm) (SpectraMax M5e, Molecular Devices). In the case of RB-BSA containing vesicles, the UV-vis spectra were background corrected by taking into account the absorbance/scattering of the polymer vesicles.

**Electron Spin Resonance Spectroscopy (ESR).** ESR measurements were performed on a Bruker CW ESR Elexsys-500 spectrometer equipped with a variable temperature unit. The spectra were recorded at 298 K with the following parameters: microwave power 2 mW, number of scans up to 20, resolution 2048 points, modulation amplitude 0.5 G. ESR spectra were simulated using the WINSIM 2002 (NIEHS/NIH) simulation package<sup>28</sup> that allows the determination of the hyperfine couplings and line width with an error of 5%.

**Flow Cytometry.**  $1 \times 10^5$  HeLa cells were seeded in a well of a 24-well plate and cultured in Dulbecco's Modified Eagle's Medium (DMEM) containing 10% fetal calf serum (FCS) for 24 h at 37 °C in a humidified CO<sub>2</sub> incubator. Then the medium was exchanged, and 100  $\mu\text{g}/\text{mL}$  polymer solution with encapsulated RB-BSA was added and incubated for another

24 h. Cells were washed with PBS, trypsinized, centrifuged, resuspended in PBS, and put on ice. Flow cytometry was measured with a BD FACSCanto II flow cytometer (BD Bioscience) using FSC and SSC detectors as well as a fluorescence channel for RB-BSA. A total of 20 000 events for each sample were analyzed, and data were processed using Flowing Software 2.5.0 (Turku Centre for Biotechnology, Finland)

**Laser Scanning Microscopy.** HeLa cells were cultured at a density of  $5 \times 10^4$  cells per well in a 8-well Lab-Tek (NalgeNunc International) for 24 h in DMEM growth medium. Afterward, 100 mg/mL nanoreactor extruded through 200, 100, and 50 nm was incubated with the cells for an additional 24 h. Then, cells were illuminated from the bottom for 25 min and washed with PBS. After staining with Hoechst 3342 (5 mg/mL) and Cell mask Deep Red (5 mg/mL) for 10 and 5 min, respectively, cells were imaged with a confocal laser scanning microscope (Carl Zeiss LSM510, Germany) equipped with a 63× water emulsion lens (Olympus, Japan). Images were recorded in multitrack mode, and the intensity of each fluorescent dye was adjusted individually: Hoechst 3342 was excited at 405 nm in channel 1, Deep Red at 633 nm in channel 2, and RB-BSA and Doxorubicin at 543 nm in channel 3. The images were recorded using Carl Zeiss LSM software (version 4.2 SP1).

**Proton Nuclear Magnetic Resonance (<sup>1</sup>H NMR).** <sup>1</sup>H NMR spectra were recorded on a Bruker DPX-400 spectrometer operated at 400 MHz in CDCl<sub>3</sub> and processed with MestReNova software. Chemical shifts are reported in ppm relative to tetramethylsilane.

**Gel Permeation Chromatography (GPC).** GPC was used in order to determine the average molecular weight  $M_n$  of the polymers and their polydispersity index (PDI). These parameters were determined using a Viscotek GPC max system equipped with four Polymer Agilent PL gel columns (10  $\mu\text{m}$  guard; mixed C; 10  $\mu\text{m}$ , 100 Å; 5  $\mu\text{m}$ , 10<sup>3</sup> Å), using chloroform as eluent at a flow rate of 1 mL min<sup>-1</sup> at 40 °C. Signals were recorded with a refractive index detector (RI) and calibrated against polystyrene standards (Agilent).

## ASSOCIATED CONTENT

### S Supporting Information

Figures S1–S6 and Tables S1, S2. This material is available free of charge via the Internet at <http://pubs.acs.org>.

## AUTHOR INFORMATION

### Corresponding Author

\*E-mail Cornelius.Palivan@unibas.ch (C.G.P.).

### Notes

The authors declare no competing financial interest.

## ACKNOWLEDGMENTS

Financial support was provided by the Swiss National Science Foundation (NRP 62 smart materials) and the National Center of Competence in Nanoscience, and this is gratefully acknowledged. We thank Prof. W. Meier from the University of Basel for providing the block copolymers. P.B. acknowledges G. Persy (University of Basel) and V. Olivieri (Microscopy Center, University of Basel) for TEM measurements. The authors thank Dr. B. A. Goodman for editing the manuscript.

## ■ REFERENCES

- (1) Freitas, R. A. Current Status of Nanomedicine and Medical Nanorobotics. *J. Comput. Theor. Nanosci.* **2005**, *2*, 1–25.
- (2) Etheridge, M. L.; Campbell, S. A.; Erdman, A. G.; Haynes, C. L.; Wolf, S. M.; McCullough, J. The Big Picture on Nanomedicine: The State of Investigational and Approved Nanomedicine Products. *Nanomedicine* **2013**, *9*, 1–14.
- (3) Najar, A.; Wu, D.; Vasquez, D.; Palivan, C. G.; Meier, W. Polymer Nanocompartments in Broad-Spectrum Medical Applications. *Nanomedicine* **2013**, *8*, 425–447.
- (4) Ohulchanskyy, T. Y.; Kopwithaya, A.; Jeon, M.; Guo, M.; Law, W.-C.; Furlani, E. P.; Kim, C.; Prasad, P. N. Phospholipid Micelle-Based Magneto-Plasmonic Nanoformulation for Magnetic Field-Directed, Imaging-Guided Photo-Induced Cancer Therapy. *Nanomedicine* **2013**, *9*, 1192–1202.
- (5) Maeda, H.; Nakamura, H.; Fang, J. The EPR Effect for Macromolecular Drug Delivery to Solid Tumors: Improvement of Tumor Uptake, Lowering of Systemic Toxicity, and Distinct Tumor Imaging in Vivo. *Adv. Drug Delivery Rev.* **2013**, *65*, 71–79.
- (6) Master, A.; Livingston, M.; Sen Gupta, A. Photodynamic Nanomedicine in the Treatment of Solid Tumors: Perspectives and Challenges. *J. Controlled Release* **2013**, *168*, 88–102.
- (7) Dougherty, T. J.; Gomer, C. J.; Henderson, B. W.; Jori, G.; Kessel, D.; Korbelik, M.; Moan, J.; Peng, Q. Photodynamic Therapy. *J. Natl. Cancer Inst.* **1998**, *90*, 889–905.
- (8) Allison, R. R.; Downie, G. H.; Cuenca, R.; Hu, X.-H.; Childs, C. J. H.; Sibata, C. H. Photosensitizers in Clinical Pdt. *Photodiagn. Photodyn. Ther.* **2004**, *1*, 27–42.
- (9) Shrestha, A.; Kishen, A. Photodynamic Therapy for Inactivating Endodontic Bacterial Biofilms and Effect of Tissue Inhibitors on Antibacterial Efficacy. *Lasers Dent. Xix* **2013**, 8566.
- (10) Hamblin, M. R.; Newman, E. L. Photosensitizer Targeting in Photodynamic Therapy 0.1. Conjugates of Hematoporphyrin with Albumin and Transferrin. *J. Photochem. Photobiol., B* **1994**, *26*, 45–56.
- (11) Konan, Y. N.; Gurny, R.; Allemann, E. State of the Art in the Delivery of Photosensitizers for Photodynamic Therapy. *J. Photochem. Photobiol., B* **2002**, *66*, 89–106.
- (12) Guo, H.; Qian, H.; Idris, N. M.; Zhang, Y. Singlet Oxygen-Induced Apoptosis of Cancer Cells Using Upconversion Fluorescent Nanoparticles as a Carrier of Photosensitizer. *Nanomedicine* **2010**, *6*, 486–495.
- (13) Roy, I.; Ohulchanskyy, T. Y.; Pudavar, H. E.; Bergey, E. J.; Oseroff, A. R.; Morgan, J.; Dougherty, T. J.; Prasad, P. N. Ceramic-Based Nanoparticles Entrapping Water-Insoluble Photosensitizing Anticancer Drugs: A Novel Drug-Carrier System for Photodynamic Therapy. *J. Am. Chem. Soc.* **2003**, *125*, 7860–7865.
- (14) Palivan, C. G.; Fischer-Onaca, O.; Delcea, M.; Itel, F.; Meier, W. Protein-Polymer Nanoreactors for Medical Applications. *Chem. Soc. Rev.* **2012**, *41*, 2800–2823.
- (15) Renggli, K.; Baumann, P.; Langowska, K.; Onaca, O.; Bruns, N.; Meier, W. Selective and Responsive Nanoreactors. *Adv. Funct. Mater.* **2011**, *21*, 1241–1259.
- (16) Kumar, M.; Grzelakowski, M.; Zilles, J.; Clark, M.; Meier, W. Highly Permeable Polymeric Membranes Based on the Incorporation of the Functional Water Channel Protein Aquaporin Z. *Proc. Natl. Acad. Sci. U. S. A.* **2007**, *104*, 20719–20724.
- (17) Ranquin, A.; Versee, W.; Meier, W.; Steyaert, J.; Van Gelder, P. Therapeutic Nanoreactors: Combining Chemistry and Biology in a Novel Triblock Copolymer Drug Delivery System. *Nano Lett.* **2005**, *5*, 2220–2224.
- (18) Langowska, K.; Palivan, C. G.; Meier, W. Polymer Nanoreactors Shown to Produce and Release Antibiotics Locally. *Chem. Commun. (Cambridge, U. K.)* **2013**, *49*, 128–130.
- (19) Baumann, P.; Balasubramanian, V.; Onaca-Fischer, O.; Sienkiewicz, A.; Palivan, C. G. Light-Responsive Polymer Nanoreactors: A Source of Reactive Oxygen Species on Demand. *Nanoscale* **2013**, *5*, 217–224.
- (20) Tanner, P.; Balasubramanian, V.; Palivan, C. G. Aiding Nature's Organelles: Artificial Peroxisomes Play Their Role. *Nano Lett.* **2013**, *13*, 2875–2883.
- (21) Axthelm, F.; Casse, O.; Koppenol, W. H.; Nauser, T.; Meier, W.; Palivan, C. G. Antioxidant Nanoreactor Based on Superoxide Dismutase Encapsulated in Superoxide-Permeable Vesicles. *J. Phys. Chem. B* **2008**, *112*, 8211–8217.
- (22) Spulber, M.; Baumann, P.; Saxer, S. S.; Pieles, U.; Meier, W. P.; Bruns, N. Poly(N-Vinylpyrrolidone)-Poly(Dimethylsiloxane)-Based Polymersome Nanoreactors for Laccase-Catalyzed Biotransformations. *Biomacromolecules* **2014**, *15*, 1469–75.
- (23) Minai, L.; Yeheskely-Hayon, D.; Yelin, D. High Levels of Reactive Oxygen Species in Gold Nanoparticle-Targeted Cancer Cells Following Femtosecond Pulse Irradiation. *Sci. Rep.* **2013**, *3*, 2146.
- (24) Ueda, A.; Hirayama, A.; Nagase, S.; Inoue, M.; Oteki, T.; Aoyama, M.; Yokoyama, H. In Vivo Detection of Intrinsic Reactive Oxygen Species Using Acyl-Protected Hydroxylamine in Puromycin Nephrosis. *Free Radical Res.* **2007**, *41*, 823–828.
- (25) Mathai, S.; Smith, T. A.; Ghiggino, K. P. Singlet Oxygen Quantum Yields of Potential Porphyrin-Based Photosensitisers for Photodynamic Therapy. *Photochem. Photobiol. Sci.* **2007**, *6*, 995–1002.
- (26) Spulber, M.; Baumann, P.; Bruns, N.; Palivan, C. G.; Meier, W. Laccase Encapsulating Polymersomes for Catalysed Biotransformation. In *SSD 12*, Bern, 2013.
- (27) Knop, K.; Mingotaud, A.-F.; El-Akra, N.; Violleau, F.; Souchard, J.-P. Monomeric Pheophorbide(a)-Containing Poly(Ethylene-glycol-B-Epsilon-Caprolactone) Micelles for Photodynamic Therapy. *Photochem. Photobiol. Sci.* **2009**, *8*, 396–404.
- (28) Stauch, O.; Schubert, R.; Savin, G.; Burchard, W. Structure of Artificial Cytoskeleton Containing Liposomes in Aqueous Solution Studied by Static and Dynamic Light Scattering. *Biomacromolecules* **2002**, *3*, 565–578.
- (29) Behera, M.; Ram, S. Spectroscopy-Based Study on the Interaction between Gold Nanoparticle and Poly(Vinylpyrrolidone) Molecules in a Non-Hydrocolloid. *Nano Lett.* **2013**, *3*, 1–7.
- (30) Spulber, M.; Schlick, S. Using Cyclodextrins to Encapsulate Oxygen-Centered and Carbon-Centered Radical Adducts: The Case of Dmpo, Pbn, and Mnp Spin Traps. *J. Phys. Chem. A* **2010**, *114*, 6217–6225.
- (31) Villamena, F. A. Superoxide Radical Anion Adduct of 5,5-Dimethyl-1-Pyrroline N-Oxide. S. Thermodynamics and Kinetics of Unimolecular Decomposition. *J. Phys. Chem. A* **2009**, *113*, 6398–6403.
- (32) Balasubramanian, V.; Onaca, O.; Ezhevskaya, M.; Van Doorslaer, S.; Sivasankaran, B.; Palivan, C. G. A Surprising System: Polymeric Nanoreactors Containing a Mimic with Dual-Enzyme Activity. *Soft Matter* **2011**, *7*, 5595–5603.
- (33) Tacar, O.; Sriamornsak, P.; Dass, C. R. Doxorubicin: An Update on Anticancer Molecular Action, Toxicity and Novel Drug Delivery Systems. *J. Pharm. Pharmacol.* **2013**, *65*, 157–170.
- (34) Ross, M. I. Intralesional Therapy with Pv-10 (Rose Bengal) for in-Transit Melanoma. *J. Surg. Oncol.* **2014**, *109*, 314–319.
- (35) Tanner, P.; Onaca, O.; Balasubramanian, V.; Meier, W.; Palivan, C. G. Enzymatic Cascade Reactions inside Polymeric Nanocontainers: A Means to Combat Oxidative Stress. *Chemistry* **2011**, *17*, 4552–4560.
- (36) Li, J. H.; Chen, Z. Q.; Huang, Z.; Zhan, Q.; Ren, F. B.; Liu, J. Y.; Yue, W.; Wang, Z. In Vitro Study of Low Intensity Ultrasound Combined with Different Doses of Pdt: Effects on C6 Glioma Cells. *Oncol. Lett.* **2013**, *5*, 702–706.
- (37) Shimizu, K.; Fujino, T.; Ando, K.; Hayakawa, M.; Yasuda, H.; Kikugawa, K. Overexpression of Oxidized Protein Hydrolase Protects Cos-7 Cells from Oxidative Stress-Induced Inhibition of Cell Growth and Survival. *Biochem. Biophys. Res. Commun.* **2003**, *304*, 766–771.
- (38) Mousavi, S. H.; Tavakkol-Afshari, J.; Brook, A.; Jafari-Anarkooli, I. Direct Toxicity of Rose Bengal in Mcf-7 Cell Line: Role of Apoptosis. *Food Chem. Toxicol.* **2009**, *47*, 855–859.
- (39) Xia, T.; Kovochich, M.; Brant, J.; Hotze, M.; Sempf, J.; Oberley, T.; Sioutas, C.; Yeh, J. I.; Wiesner, M. R.; Nel, A. E. Comparison of the Abilities of Ambient and Manufactured Nanoparticles to Induce

Cellular Toxicity According to an Oxidative Stress Paradigm. *Nano Lett.* **2006**, *6*, 1794–1807.

(40) Nardin, C.; Thoeni, S.; Widmer, J.; Winterhalter, M.; Meier, W. Nanoreactors Based on (Polymerized) Aba-Triblock Copolymer Vesicles. *Chem. Commun. (Cambridge, U. K.)* **2000**, 1433–1434.

(41) Nardin, C.; Hirt, T.; Leukel, J.; Meier, W. Polymerized Aba Triblock Copolymer Vesicles. *Langmuir* **2000**, *16*, 1035–1041.

(42) Tanner, P.; Balasubramanian, V.; Palivan, C. G. Aiding Nature's Organelles: Artificial Peroxisomes Play Their Role. *Nano Lett.* **2013**, *13*, 2875–2883.

(43) Serrander, L.; Cartier, L.; Bedard, K.; Banfi, B.; Lardy, B.; Plastre, O.; Sienkiewicz, A.; Forro, L.; Schlegel, W.; Krause, K.-H. Nox4 Activity Is Determined by mRNA Levels and Reveals a Unique Pattern of Ros Generation. *Biochem. J.* **2007**, *406*, 105–114.